Sensitivity of sea ice to physical parameterizations in the GISS global climate model

Jiping Liu,[1,2] Gavin A. Schmidt,[3] Douglas G. Martinson,[2,4] David Rind,[1,2] Gary Russell,[1] and Xiaojun Yuan[4]

Received 5 October 2001; revised 6 September 2002; accepted 6 November 2002; published 27 February 2003.

[1] The GISS coupled model is used to investigate the sensitivity of sea ice to each of the following parameterizations: (1) two sea ice dynamics (CF: cavitating fluid; VP: viscous-plastic), (2) the specification of oceanic isopycnal mixing coefficients in the Gent and McWillams isopyncal mixing (GM), and (3) the wajsowicz viscosity diffusion (WV). The large-scale sea ice properties are highly sensitive to sea ice dynamics. With the inclusion of resistance to shear stress, VP captures the major observed sea ice drift features and improves the simulations of sea ice concentrations, thickness, and export through Fram Strait relative to CF. GM significantly improves the simulation of vertical temperature distributions in the Southern Ocean, although it leads to a dramatic reduction of Antarctic sea ice cover. The reduced oceanic isopycnal mixing coefficients lead to Arctic sea ice that tends to be less and thinner in almost the entire Arctic except in the North Pacific and Labrador Sea, while Antarctic sea ice that extends more equatorward throughout the circumpolar regions. The responses of sea ice to WV show an enlargement and thickening of sea ice in the Arctic, within the ice packs around the Antarctic and a reduction and thinning of sea ice in the northern Weddell and Ross Seas. On the basis of these experiments, two composite experiments with the best parameterizations are investigated. The atmospheric responses associated with sea ice changes are discussed. While improvements are seen, there are still many unrealistic aspects that will require further improvements to sea ice and ocean components. *INDEX TERMS:* 4207 Oceanography: General: Arctic and Antarctic oceanography; 4255 Oceanography: General: Numerical modeling; 4540 Oceanography: Physical: Ice mechanics and air/sea/ice exchange processes; *KEYWORDS:* sea ice sensitivity to physical parameterizations

Citation: Liu, J., G. A. Schmidt, D. Martinson, D. H. Rind, G. L. Russell, and X. Yuan, Sensitivity of sea ice to physical parameterizations in the GISS global climate model, *J. Geophys. Res.*, *108*(C2), 3053, doi:10.1029/2001JC001167, 2003.

1. Introduction

[2] Sea ice plays an important role in the determination of regional and global climate through dynamic and thermodynamic processes and various feedback mechanisms [*Walsh*, 1983]. First, the high albedo of sea ice substantially reduces the solar radiation absorbed by the polar regions. Second, sea ice has a strong insulating effect on the underlying ocean drastically reducing the exchange of heat, moisture and momentum between the atmosphere and the ocean. Third, sea ice strongly influences the global thermohaline circulation through the impacts on the fresh water budget and dense water formation. Because the albedo, insulating and density effects are so strong, even small changes in the amount of sea ice cover might be expected to drive large changes in the regional and ultimately global climate [*Parkinson et al.*, 2001].

[3] However, while sea ice is important in the global climate system, sea ice dynamic, and thermodynamic processes have been historically oversimplified in global climate models [*Randall et al.*, 1998]. *Rind et al.* [1995] showed that feedbacks associated with sea ice variability accounts for over one third of the double CO_2 global warming in the Goddard Institute of Space Studies (GISS) general circulation model (GCM) coupled with a q-flux ocean [*Hansen et al.*, 1983], which further indicates the importance of incorporating realistic sea ice processes in global climate models. Moreover, the impacts of subgrid scale ocean processes on sea ice simulations have not received much attention in global climate modeling. For instance, climate change simulations often show a hemispheric asymmetry with more warming in the northern high latitudes than in the south [*Kattenberg et al.*, 1996], however a recent Canadian Center for Climate Modeling and Analysis (CCCma) experiment using the *Gent et al.* [1995] and *Gent and McWilliams* [1990] isopycnal mixing relative

[1]NASA/Goddard Space Flight Center, Institute for Space Studies, New York, New York, USA.
[2]Department of Earth and Environmental Sciences, Columbia University, Palisades, New York, USA.
[3]Center for Climate Systems Research, Columbia University, New York, New York, USA.
[4]Lamont-Doherty Earth Observatory of Columbia University, Palisades, New York, USA.

Copyright 2003 by the American Geophysical Union.
0148-0227/03/2001JC001167$09.00

to the horizontal/vertical diffusion exhibits a much more symmetric warming [*Flato and Boer*, 2001]. This indicates that the sensitivity of the high-latitude ocean characteristics to climate change is sensitive to subgrid scale ocean physical parameterizations. The IPCC assessment [*Gates et al.*, 1996] also showed that the largest disagreement among global climate model simulations of present and future climate is in the polar regions. This disagreement among the models is not only due to differing atmospheric circulation [*Bitz et al.*, 2001] but also to dramatically different sea ice treatments. These facts reflect our limited understanding of the sensitivity of sea ice to sea ice and subgrid scale ocean processes, and the model's ability to represent complex air-sea-ice interactions.

[4] Therefore it is desirable to investigate the impacts of more sophisticated sea ice and subgrid scale ocean processes on sea ice simulations in global climate models. Although these physical parameterizations have been examined in stand alone or regional models and forced by observed forcings or coupled with simple atmosphere and/or ocean models, problems that are relatively minor in stand-alone or regional models can be quickly amplified when the different components interact in fully coupled models [*Weatherly et al.*, 1998]. Thus it is important to identify the parameterizations that improve the overall simulations of sea ice in global climate models whenever possible.

[5] In order to address these concerns, we performed several sensitivity studies (Table 1) using the GISS global climate model [*Russell et al.*, 1995, 2000]. In particular, we discuss the roles of the cavitating fluid [*Flato and Hibler*, 1992] and viscous-plastic sea ice dynamics [*Zhang and Hibler*, 1997; *Zhang and Rothrock*, 2000], Gent and McWilliams isopycnal mixing [*Gent and McWilliams*, 1990; *Gent et al.*, 1995] and associated oceanic isopycnal mixing coefficient specification [*Visbeck et al.*, 1997] and Wajsowicz viscosity diffusion [*Wajsowicz*, 1993] in determining sea ice simulations. On the basis of these experiments we then performed two composite experiments, which combine the best parameterizations in order to see the accumulative effects.

2. Model Description and the Control Run

[6] The atmospheric component of the GISS coupled model [*Russell et al.*, 1995, 2000] is similar to that of *Hansen et al.* [1983] except that atmospheric conservation equations for mass and momentum are solved on an Arakawa C grid instead of the B grid as formerly used, and advection of potential enthalpy and water vapor uses a linear upstream scheme [*Russell and Lerner*, 1981]. Unlike rigid-lid ocean models, the present ocean model conserves mass and not volume, has a free surface and does not use the Boussinesq approximation, applies the linear upstream scheme for the advection of potential enthalpy and salt, and employs the KPP vertical mixing scheme of *Large et al.* [1994]. The horizontal resolution for both the atmosphere and ocean component is 4° in latitude by 5° in longitude, with nine vertical layers in the atmosphere and 13 vertical layers in the ocean. The use of the linear upstream scheme in both components allows the model to calculate both the mean and first-order gradient of tracers (heat and water vapor in the atmosphere as well as heat and salt in the ocean) in three dimensions. This approach effectively provides the model finer horizontal and vertical resolution, when calculating subgrid scale processes such as atmospheric condensation and ocean vertical mixing. A polar filter is used to treat the convergence of grid points along meridians for numerical stability [*Arakawa and Lamb*, 1977]. Owing to the singularity of the poles the polar grid box is treated as a homogeneous region by averaging the north-south exchanges across the latitude next to the poles. The model also transports mass, heat, and salt through 12 subgrid scale straits. Continental runoff and glacial ice melting eventually find their way back to the oceans via a river network [*Miller et al.*, 1994]. Atmospheric and oceanic surface fluxes are solved and applied synchronously. The model does not use flux adjustments.

[7] The grid resolution of the sea ice component is identical to that of the atmosphere and ocean components. In the control run the sea ice dynamics follows the cavitating fluid rheology of *Flato and Hibler* [1992]. A linear upstream scheme is used to advect sea ice. The thermodynamic sea ice component conserves mass and energy and involves four vertical layers. Sea ice cover is determined by energy exchange with the atmosphere and the ocean. Surface fluxes calculated from the atmospheric model cause the mixed layer in the open ocean fraction to cool to the freezing point and form sea ice subsequently with minimum thickness (0.2 m) and areal concentration required to conserve energy. If the ice-ocean fluxes in the sea ice covered fraction extract sufficient heat from the ocean to cool the mixed layer to the freezing point, subsequent cooling causes sea ice to thicken. In essence, the first layer of the ocean model is kept at its freezing point in the presence of sea ice. A more sophisticated boundary layer formulation at the base of sea ice [*McPhee et al.*, 1987; *Holland and Jenkins*, 1999] that allows a temperature gradient at the base of sea ice is currently being tested. If the horizontal open ocean fraction becomes less than a calculated lead fraction (0.06 divided by sea ice thickness), then sea ice cover is contracted horizontally to meet this calculated lead fraction and increases its thickness (conserving mass and energy). Sea ice contains no salt, which increases the salinity of the uppermost ocean layer as sea ice grows thermodynamically. Snow is considered in the first thermal layer and can be compacted into ice as a function of snow thickness, rainfall, and melt. The spectrally integrated albedo over sea ice varies from 0.44 for sea ice without snow to 0.84 for sea ice covered by deep snow.

[8] The original GISS coupled model generates too excessive Antarctic sea ice due to much colder and fresher upper ocean water in the Southern Ocean, which might be related to excessive glacial ice calved into the Southern Ocean [*Liu et al.*, 2002]. For the control run used in this paper we reduce the glacial ice discharge in the Antarctic based on the IPCC report [*Intergovernmental Panel on Climate Change* (*IPCC*), 1995]. Compared with the original control run, our control run did indeed improve the sea ice and high-latitude ocean vertical temperature and salinity structure simulations to some degree (not shown). Seven sensitivity experiments are listed in Table 1 (see detailed discussion in section 4). Each experiment was run for 30 years, starting with the atmospheric state from National Meteorological Center Data sets, the Levitus ocean temperature and salinity distributions [*Levitus and Boyer*, 1994; *Levitus et al.*, 1994],

Table 1. Sensitivity Experiments

Abbreviation	VP	GM	GMv1	GMv2	WV	C1	C2
Experiment	Viscous-Plastic sea ice rehology	Gent and McWilliams isopycnal mixing	GM with original Visbeck mixing coefficient	GM with doubled Visbeck mixing coefficient	Wajsowicz viscosity diffusion	VP + GMv1 +WV	VP + GMv2 + WV

and sea ice conditions from *Walsh and Johnson* [1979] for the Northern Hemisphere and *Alexander and Mobley* [1976] for the Southern Hemisphere, which are the same as that employed by *Russell et al.* [2000] for simulations of the next century. Results are shown for the average over the last 10-year of the model simulation. For a 40-year control run, the similarity between the 3rd 10-year averages and the 4th 10-year averages (Table 2) shows that 30-year simulations are generally sufficient to establish the first order (dynamic and hydrologic) differences between the control run and each sensitivity experiment in the polar regions.

3. Data

[9] Several remotely sensed and observational data sets have been used for comparison with the model results in this paper. Remotely sensed sea ice drift (W. Emery et al., personal communication, 2001) and concentrations retrieved from SMMR/SSMI (the Nimbus-7 Scanning Multichannel Microwave Radiometer and Spatial Sensor Microwave Imagers) over the period of 1979–1999 are used. The satellite derived monthly mean ice motions are used in order to compare the large-scale velocity patterns, since the coverage of buoys is limited. The monthly mean ice concentrations for these years are interpolated to the GISS model grid for comparisons. Surface air temperature (SAT) from NCEP/NCAR reanalysis is annually and seasonally averaged over the period 1958–1980 and compared with the model results. The observational data SAT after 1980 is not included, since the strong warming during the last two decades would shift the climatology.

4. Sensitivity Experiment Implementation and Results

4.1. Sensitivity to Sea Ice Dynamics

[10] The important role of sea ice dynamics in the climate system has been shown by model simulations. Experiments with stand-alone sea ice models [*Hibler*, 1984; *Lemke et al.*, 2000] have demonstrated that sea ice thermodynamics-only models are more sensitive to changes in the thermal forcing than those which include sea ice dynamics. Similarly, GCMs appear to be less sensitive to global warming induced by double CO_2 when sea ice dynamics are included [*Pollard and Thompson*, 1994]. Dynamic modeling of sea ice is based on the principles of the conservation of the mass and momentum and requires knowledge of the forces acting on the ice floes. These include the Coriolis effect, air and water drags, gravitational pull due to the sea surface tilt, and the internal sea ice stress resulting from the interaction between different ice floes. Relative to the first four forces, the best way to model the internal ice stress is less clear and many different approaches have been proposed. Recently, four sea ice dynamic parameterizations ((1) simple free drift with velocity correction, (2) compressible Newtonian fluid, (3) cavitating fluid, and (4) viscous-plastic rheology) have been evaluated in a sea ice model for the Arctic with the same NCEP/NCAR atmospheric forcings, thermodynamic formulation, and parameterizations [*Kreyscher et al.*, 2000] (Sea Ice Model Intercomparison Project (SIMIP)). Overall, the viscous-plastic rheology [*Hibler*, 1979; *Hibler and Schulson*, 1997] (hereafter referred as VP) yields the most realistic simulations. The GISS coupled model originally modeled the sea ice as a cavitating fluid [*Flato and Hibler*, 1992] (hereafter referred as CF), in which sea ice is assumed to have plastic behavior in the case of compressive deformation and allows divergence without any internal stress. In this study, we replaced it with a computationally efficient VP rheology [*Zhang and Hibler*, 1997; *Zhang and Rothrock*, 2000] to investigate the sensitivity of sea ice simulations to different sea ice dynamics. The main difference between CF and VP is that CF has no resistance to shear stress between ice floes, while VP does. Since the GISS ocean model has a free ocean surface, the surface slope in the momentum equation is calculated based on the simulated gradient of surface dynamic height, instead of calculated from the geostrophic ocean current assumption by *Zhang and Rothrock* [2000].

Table 2. Annual Averaged SAT, Sea Ice Thickness, and Area[a]

	SAT, °C		Thickness, m		Area, 10^6 km^2	
Run	(45°N–90°N, sea ice and ocean)	(90°S–45°S, sea ice and ocean)	NH	SH	NH	SH
Control	−7.92 (−7.59)	−1.06 (−0.93)	1.66 (1.56)	0.24 (0.26)	10.96 (10.51)	7.87 (7.90)
VP	−9.75	−1.53	2.36	0.32	11.75	9.21
GM	−8.91	0.89	1.97	0.16	11.36	3.45
GMv1	−8.31	−0.69	1.77	0.23	11.19	7.09
GMv2	−8.48	0.17	1.73	0.19	11.07	5.16
WV	−10.75	−1.45	2.22	0.29	12.98	8.59
C1	−11.54	−1.96	3.26	0.37	12.9	10.28
C2	−11.2	−1.21	3.13	0.33	12.77	8.42
Obs	−8.63	−2.33	2.66		11.49	9.72

[a]The 4th 10-year averages of the control run are shown in parentheses.

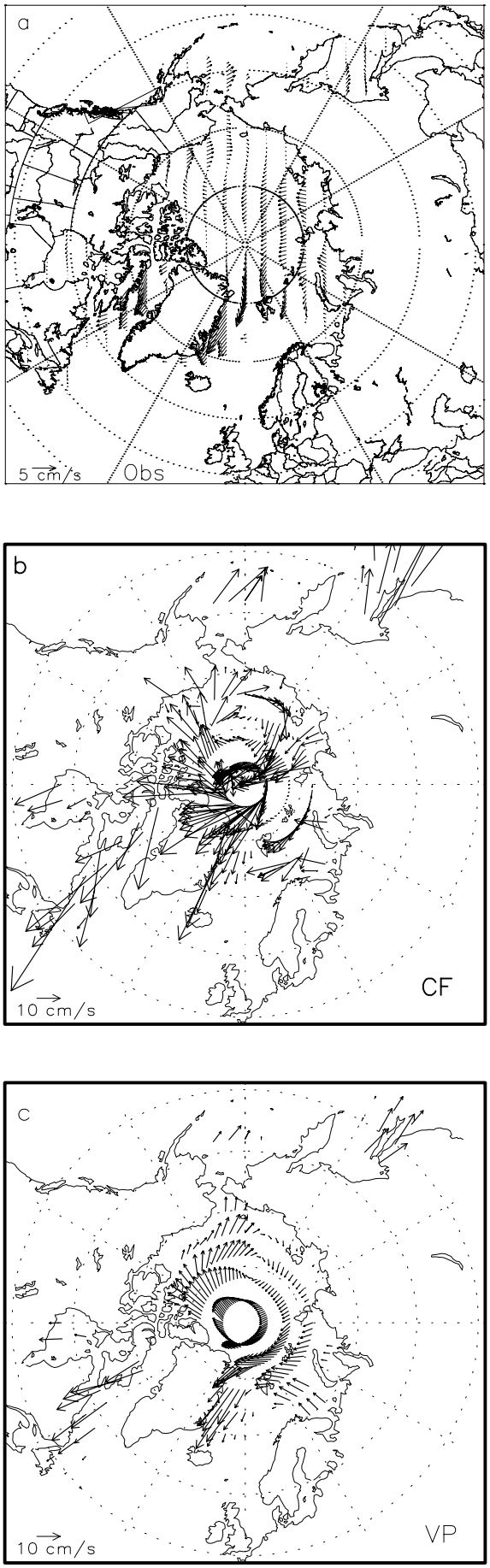

[11] Figure 1 shows the February (winter maximum sea ice extent) sea ice drift in the Arctic. Qualitatively speaking, VP captures major observed features (Figure 1a): (1) A large amount of the sea ice leaves the Arctic Ocean through Fram Strait; (2) the Beaufort Gyre drives the sea ice in an anticyclonic motion out of the Beaufort Sea, then merges with the sea ice from the eastern Siberian coast into the Transpolar Drift Stream (TDS). However, the Beaufort Gyre is broader and the center of the gyre is located northward (near the North Pole) from its climatology (Figure 1c). Higher horizontal resolution models might be desired to improve the representation of the Beaufort Gyre by more faithfully resolved passages, coastlines, and islands. Differences between CF and VP are clearly visible. The ice drift is far too large in CF due to the absence of shear stress (Figure 1b), while VP gives ice drift that is more reasonable but still almost two times larger than the observations. Additionally, VP produces a more continuous TDS than CF.

[12] In the Antarctic the simulated September (winter maximum sea ice extent) sea ice drift in CF and VP capture most observed features: (1) The coastal westward ice drift and eastward ice drift in the Antarctic Circumpolar regions, (2) the cyclonic ice circulation in the Weddell and Ross Seas, (3) the strong northward ice flow along the Antarctic Peninsula and in the Ross Sea itself, which are in agreement with the synoptic patterns and katabatic flow in these regions (Figures 2a, 2b, and 2c). The ice drift in VP is again almost two times larger than the observations, but it is much larger in CF (especially along the coastlines). However, since the ice drift derived from the satellites has been shown to underestimate the drift speed in the Antarctic by as much as half [*Weatherly and Zhang*, 2001], VP may in fact give reasonable results.

[13] Figure 3 shows the monthly mean ice drift-speed distributions. The error of the drift characteristics is measured by the root mean square (rms) of speed distribution differences between each simulation and the observations. The RMS in CF is larger than that of VP for four cases below. For the Arctic, the RMS is 9.2% and 6.8% in February and 8.3% and 5.4% in September. For the Antarctic, the RMS is 10.3% and 6.7% in September and 2.9% and 2.6% in February. *Weatherly et al.* [1998] also reported the excessive sea ice drift in CF in the NCAR Climate System Model. Compared with the shape of the observed drift-speed histogram in the Arctic and Antarctic (tail off at less than 10 cm/s), the drift-speed histogram in CF has a very long tail-off at ~55 cm/s, while the tail ends at ~20–25 cm/s in VP. Again, VP obviously improves the simulation of ice drift in both hemispheres. Since the ice-ocean drag coefficient decreases linearly with ice thickness in CF, while it is a constant in VP, we tested the role of the constant ice-ocean drag coefficient in CF. The results suggest that the ice velocities in CF (especially at the marginal ice zones in the Arctic and along the coastlines of the Antarctic) are only

Figure 1. (opposite) The (a) Arctic observed (derived from the satellite SMMR/SSMI sensors) and simulated monthly mean sea ice drift (cm/s) in February for the (b) control (cavitating fluid) and (c) viscous-plastic runs. Note the different scale vectors in the observations and model simulations.

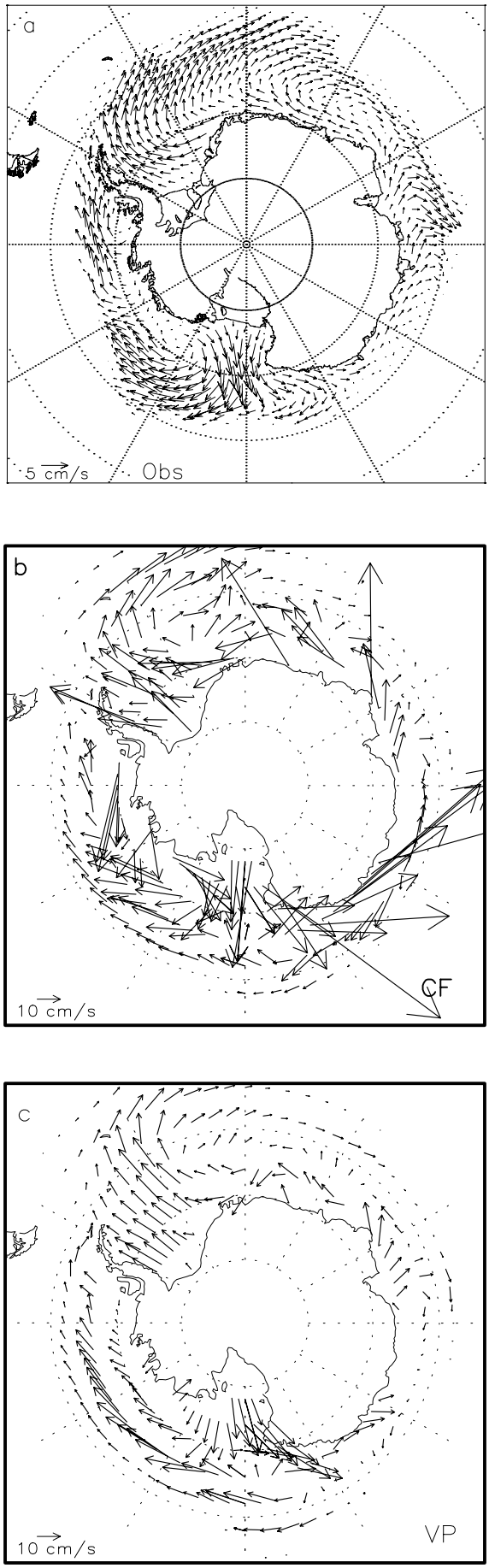

slightly attributed to the specification of the ice-ocean drag coefficient. This leaves the inclusion of the resistance to shear stress as the primary cause of the improvements of ice drift simulations. Additionally, the simulated surface wind is also relatively large in these regions.

[14] The Arctic sea ice concentrations in February (Figure 4) and September (not shown) show that ice cover is more extensive in CF (control run) as compared with the observations. There is ice cover in the Barents Sea in February and September and in the North Pacific and Labrador Sea in February, none of which should have significant ice cover. VP tends to reduce ice cover in the North Pacific and Labrador Sea in February. Additionally, there is an enlargement of sea ice in the eastern Arctic with a maximum (~20–30%) in the northern GIN Seas (Greenland-Iceland-Norwegian) and a reduction of sea ice in the Beaufort Sea in February and September.

[15] The simulated September (Figure 5) and February (not shown) sea ice concentrations in the Antarctic show excessive northward extension in CF relative to the observations. The February ice cover in CF exhibits a more gradual gradient at the sea ice edges, with lower concentrations within the ice packs around the Antarctic. In February, VP produces more sea ice between the southern Weddell Sea and the western Indian sector of the Antarctic and in the Ross Sea (~10–30%), with less sea ice along the outermost circumpolar regions, which tend to increase the gradient at the sea ice edges. In September, VP generates more sea ice (~20–40%) against the Antarctic Peninsula and western Ross Sea than CF does.

[16] The annual mean sea ice thickness is shown in Figure 6. CF does not produce the observed pressure-ridged thickness buildup against the northern Greenland Sea and off the Canadian Archipelago [*Bourke and Garrett*, 1987]. Sea ice in CF is also much thinner than that of the observations for almost the entire Arctic, except the Eurasian Basin. One reason is that the absence of shear stress in CF prevents the pileup of sea ice against the northern Greenland coast and off the Canadian Archipelago. Another reason might be that the model's sea ice transport through the Canadian Archipelago is too high, primarily because the passages are too wide in the GISS coupled model [*Miller and Russell*, 2000]. Relative to CF, VP improves the annual mean ice thickness by a thickening of sea ice in the eastern Arctic as well as in the northern Greenland Sea and along the Eastern Greenland Coast (~0.8–1.6 m) and limits a southward ice extension somewhat by a thinning of sea ice in the North Pacific and Labrador Sea. However, the ice thickness distribution pattern is not much improved.

[17] In the Antarctic the annual mean sea ice thickness is primarily ~0.2–0.4 m, with a buildup of near 1 m in CF against the western Ross Sea and Antarctic Peninsula (Figure 7). VP increases ice thickness along the coastlines, especially in the aforementioned two ice buildup regions to

Figure 2. (opposite) The (a) Antarctic observed (derived from the satellite SMMR/SSMI sensors) and simulated monthly mean sea ice drift (cm/s) in September for the (b) control (cavitating fluid) and (c) viscous-plastic runs. Note the different scale vectors in the observations and model simulations.

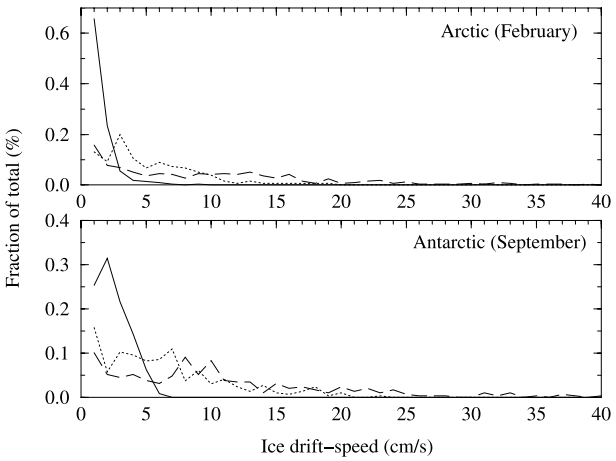

Figure 3. The observed (solid line) and simulated (dashed line: cavitating fluid; dotted line: viscous-plastic) monthly mean ice drift-speed distributions in February for the Arctic and in September for the Antarctic.

1.5 m. This is in general agreement with values from the sparse observations [*Harder and Lemke*, 1994]. Additionally, VP decreases ice thickness in the Bellingshausen and Amundsen Seas, the western Pacific sector of the Antarctic, and the northeast Weddell Sea.

[18] Sea ice export through Fram Strait is believed to be an important diagnostic of the mass and energy budgets of the Arctic Ocean and has a great impact on the global thermohaline circulation [*Aagaard and Carmack*, 1989; *Harder et al.*, 1998; *Hilmer et al.*, 1997]. The monthly ice volume exports through Fram Strait are calculated for a zonal section at 79°N from the northeastern tip of Greenland to the northwestern tip of Spitsbergen. The annual mean ice outflow is 2039 km^3/yr in the VP approach, which is 3.5% higher than that of the CF approach (1970 km^3/yr) and slightly closer to the observations (2366 km^3/yr) [*Kwok and Rothrock*, 1999]. Both CF and VP have an appropriate seasonal cycle, although the magnitude of the ice outflow is too low in summer relative to the observations (not shown). Although the annual mean ice outflow in CF does not deviate too far from the observations, it should be noted that it is the product of too high ice velocity and too low ice thickness. The value of VP by contrast is a result of reasonable ice velocity and thickness.

4.2. Sensitivity to Subgrid Scale Ocean Physical Parameterizations

[19] The important role of high-latitude upper ocean characteristics in the maintenance and variability of sea ice has become increasing clear. For example, numerous studies show that the recent thinning of sea ice in the central Arctic is related to the loss of the cold halocline layer [*Steele and Boyd*, 1998; *Martinson and Steele*, 2001]. In the Antarctic the combination of diffusive and entrainment heat fluxes are sufficient to supply nearly all of the winter air-sea heat flux, keeping net winter sea ice thickness growth to negligible levels [*Martinson*, 1990]. Therefore the effects of subgrid scale ocean physical parameterizations, which can radically change upper ocean characteristics, must be evaluated on their effects on sea ice as well as their general effects on the ocean temperature and salinity profiles.

4.2.1. Isopycnal Mixing Tracer and Thickness Diffusion

[20] Energetic mesoscale eddies contribute the mixing of density, tracers, and momentum along isopycnals as well as diffusing isopycnal thickness itself, which play an important role in the dynamics of ocean circulation. It is common to simulate the interaction between mesoscale eddies and the wind driven general circulation with an adiabatic approximation. Resulting density fields are spatially smooth and isopycnal surfaces do not undergo overturning and breaking motions. Analyses from the eddy-resolving ocean models show that the divergence of the mean density flux by mean velocity is balanced by the divergence of mean density flux due to mesoscale eddies. However, that balance is not developed in coarse resolution ocean models. The Gent and McWilliams isopycnal mixing [*Gent and McWilliams*, 1990; *Gent et al.*, 1995] (hereafter referred as GM) is a scheme that preserves the important properties of adiabatic evolution and mimics mesoscale eddy isopycnal mixing. Their parameterization is based on down gradient diffusion of tracer anomalies along isopycnal surfaces and a mixing of isopycnal thickness. The latter can be viewed as a representation of eddy induced transport, and therefore the parameterization has both a diffusive and an advective component, each being associated with one mixing coefficient. In all following discussions we take these coefficients to be equal. Thus tracers are advected by the effective transport velocity, which is the sum of the large-scale velocity and the eddy-induced transport velocity. *Danabasoglu et al.* [1994] and *Danabasoglu and McWilliams* [1995] have shown that the use of the GM scheme appears to improve the performance of the ocean circulation in coarse resolution ocean models.

[21] While the GM scheme makes an important improvement on how mesoscale eddies affect the ocean circulation, it is unclear whether the mixing coefficients (k_m) are a function of space and time. Although the GM scheme is usually implemented with a uniform value of the two mixing coefficients, eddy activity is known to have a wide range of spatial and temporal variations [e.g., *Schmitz*, 1996]. Therefore the specification of an appropriate k_m that reflects such variations in eddy activity is necessary. *Held and Larichev* [1996] suggest that the GM scheme would be improved if a spatially nonuniform k_m is introduced based on some idealized simulations of geostrophic turbulence. *Visbeck et al.* [1997] proposed that k_m is proportional to, λ^2/T, where λ is the radius of deformation and T is the Eady timescale from the growth of unstable baroclinic waves. Recent analysis of *Bryan et al.* [1999] shows that the idea proposed by *Visbeck et al.* [1997] provided a better representation of mesoscale eddy activities in the western boundary and Antarctic Circumpolar Current.

[22] Thus we investigate the sensitivity of sea ice and high latitude ocean characteristics in the GISS coupled model to (1) the GM scheme with constant mixing coefficients (GM), (2) the original (GMv1), and (3) doubled (GMv2) Visbeck scaling mixing coefficients. In all cases the GM scheme was implemented in line with the skew flux formulation developed by *Griffies et al.* [1998].

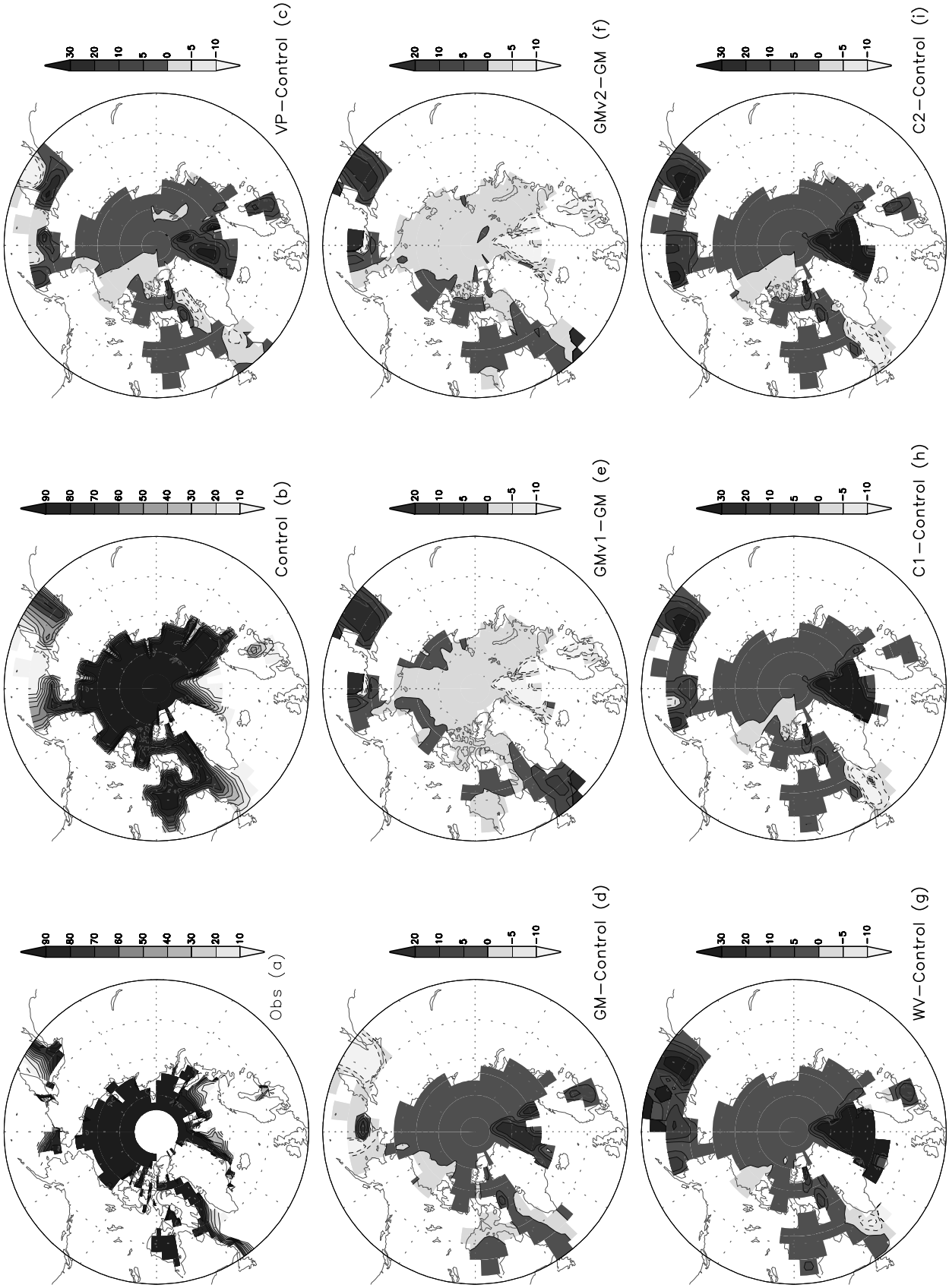

Figure 4. Arctic sea ice concentrations (%) for the (a) observations and the (b) control run, differences between VP, GM, WV, C1, C2 and Control (c, d, g, h, i), difference between GMv1, GMv2 and GM (e, f) in February.

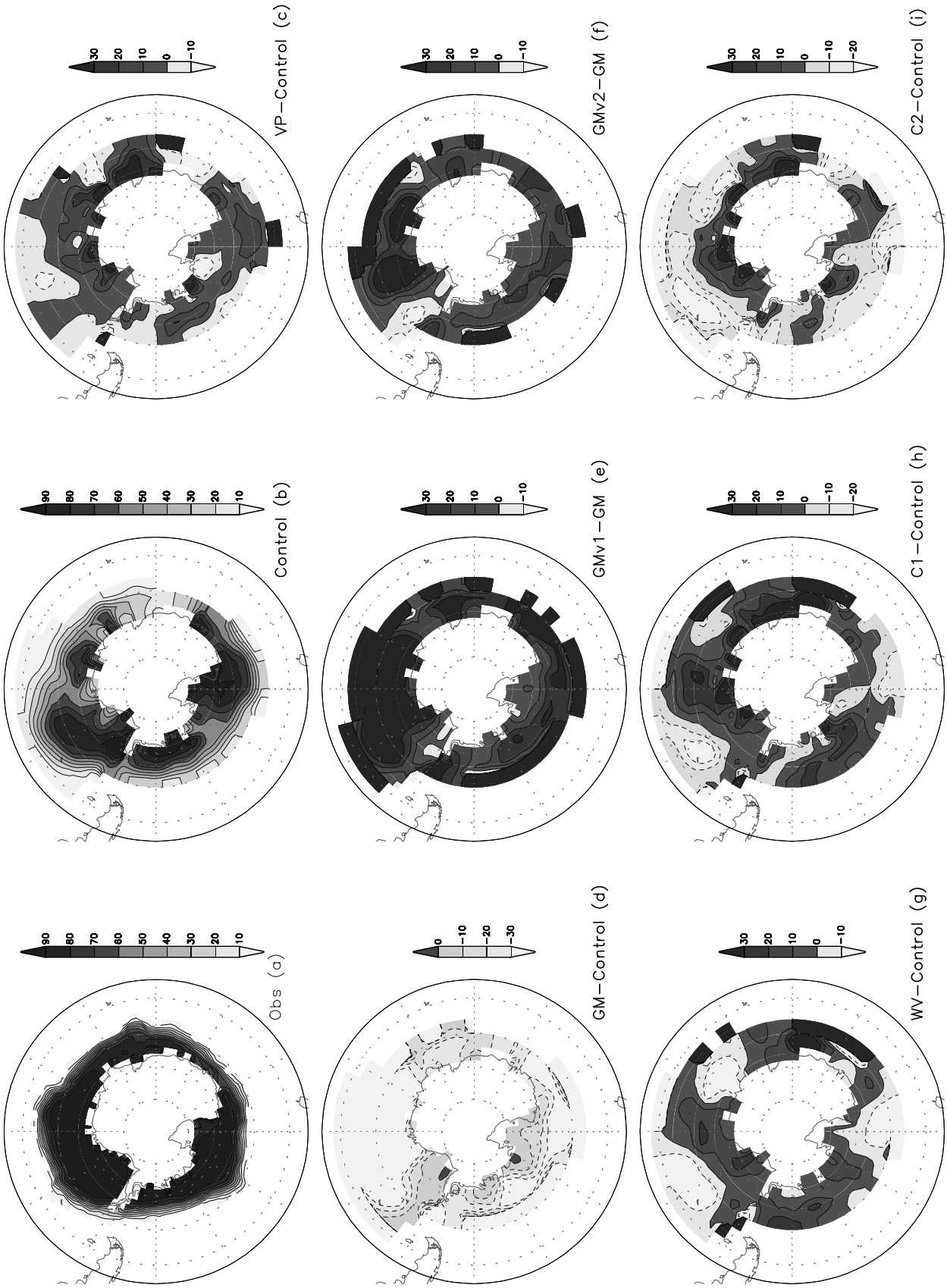

Figure 5. Antarctic sea ice concentrations (%) for the (a) observations and the (b) control run, differences between VP, GM, WV, C1, C2 and Control (c, d, g, h, i), difference between GMv1, GMv2 and GM (e, f) in September.

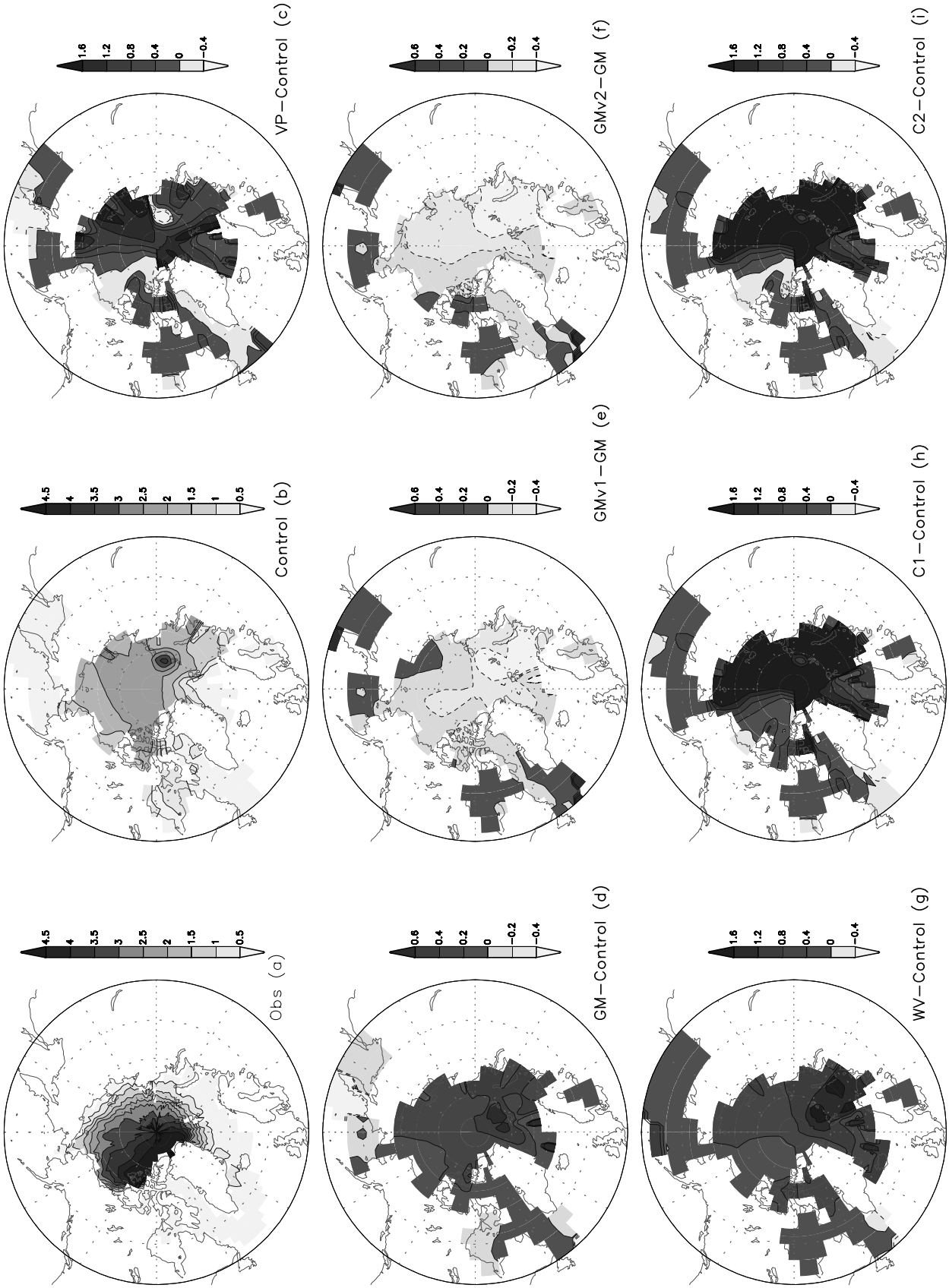

Figure 6. Arctic annual mean sea ice thickness (m) for the (a) observations and the (b) control run, differences between VP, GM, WV, C1, C2 and Control (c, d, g, h, i), difference between GMv1, GMv2 and GM (e, f).

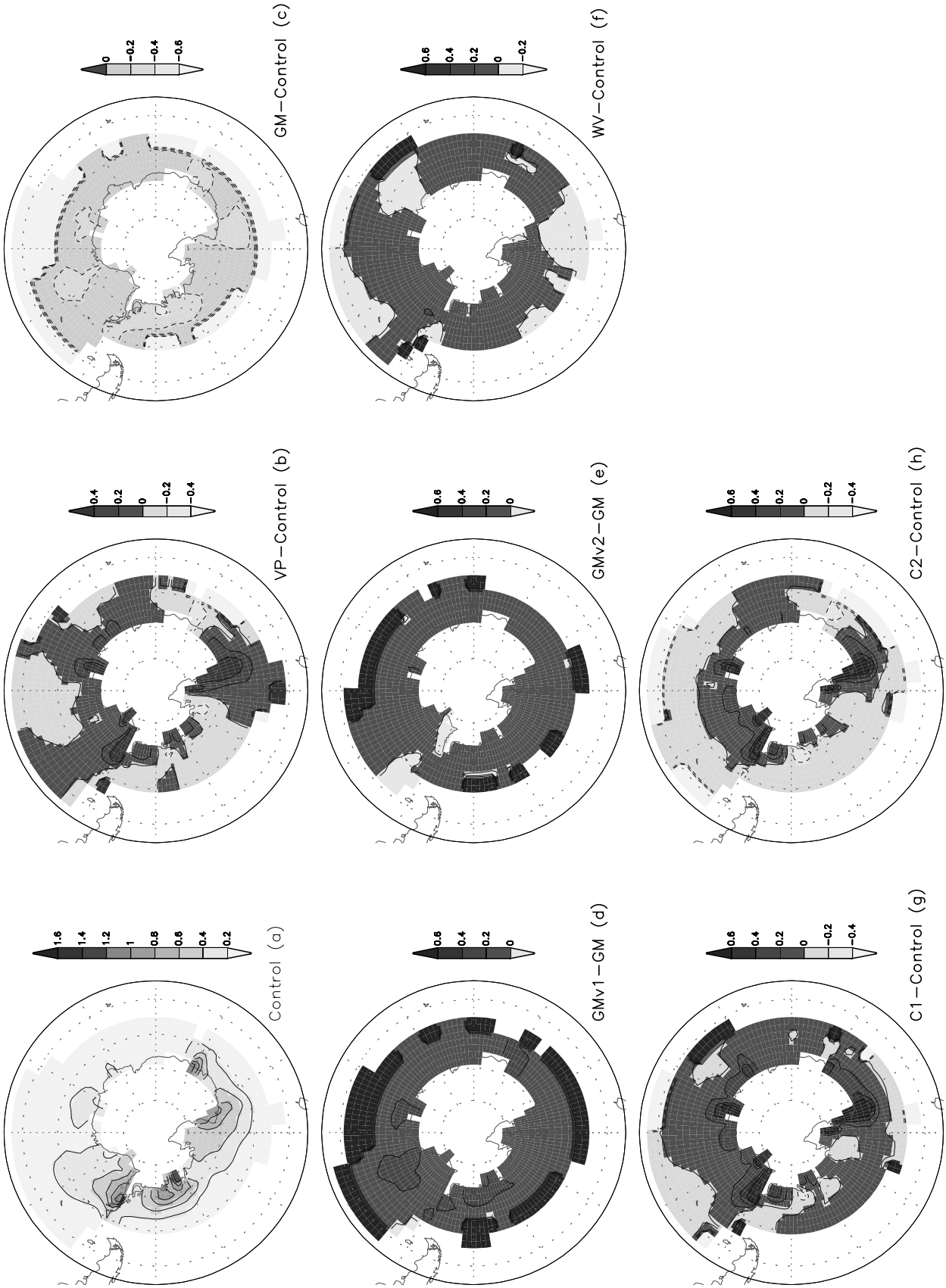

Figure 7. Antarctic annual mean sea ice thickness (m) for the (a) control run, differences between VP, GM, WV, C1, C2 and Control (b, c, f, g, h), difference between GMv1, GMv2 and GM (d, e).

Compared with the uniform k_m (1000 m^2/s) in GM, the spatial distribution of the Visbeck k_m in the GISS coupled model shows comparable k_m along passages and coastlines and smaller k_m in the interior of the Arctic in GMv1. The Visbeck k_m gradually decreases from the midlatitude to high latitude with an average of 172 m^2/s south of 50°S in GMv1. The mixing coefficients in GMv2 are roughly doubled values everywhere relative to that of GMv1 (implying that the radius of deformation and Eady timescale are not much effected by the GM scheme).

[23] The sea ice concentration differences in the Arctic between the control run and the GM run show that ice cover increases for almost the entire Arctic Ocean in February (Figure 4) and September (not shown), while decreases in the North Pacific and Labrador Sea in February. With the reduced mixing coefficients from GM through GMv2 to GMv1, in general, ice cover decreases in almost the entire Arctic Ocean in February and September, while increases in the North Pacific and Labrador Sea in February but in nonlinear way.

[24] Relative to the control run, the sea ice cover retreats significantly for the entire Antarctic in September (Figure 5), while only in the western Antarctic in February (since the eastern Antarctic is almost ice free, not shown) in the GM run. The largest reduction of sea ice can be ~30% from the control run to the GM run. With the reduced mixing coefficients from GM through GMv2 to GMv1, sea ice extends more equatorward around the entire Antarctic in September and the western Antarctic in February and tends to be more along the coastlines.

[25] Compared with the control run, the changes of the annual mean Arctic and Antarctic sea ice thickness from GM through GMv2 to GMv1 show similar features to the changes of ice cover in the Arctic and Antarctic from GM through GMv2 to GMv1 (Figures 6 and 7).

[26] The more and thicker sea ice in the Arctic in GM, GMv1, and GMv2 relative to the control run can not easily be explained by the vertical ocean temperature and salinity profiles, since these profiles change little compared to the control run (not shown). Rather, sea ice responses can be explained by the decreases in both the poleward oceanic and atmospheric heat transports. North of 52°N, the oceanic heat transports are reduced by 0.09, 0.06, and 0.05 PW in GM, GMv2, and GMv1, respectively, while the atmospheric heat transports are reduced by 0.05, 0.11, and 0.18 PW in GM, GMv2, and GMv1, respectively, compared with the control run. The similarity of sea ice changes in GMv1 and GMv2 suggests that the oceanic heat transports might have a larger influence on sea ice than the atmospheric counterpart, since these two schemes have similar oceanic heat transport decreases relative to the quite different decreases in atmospheric heat transports.

[27] Figure 8 shows the observed [*Levitus and Boyer*, 1994] and simulated September ocean temperature profiles along 107.5°W and 32.5°W of the Southern Ocean. The slope of the isotherms decreases from the control run, through GMv1, GMv2, to GM, which works to spread the upper warm water southward and shifts the zone of weak vertical stability southward. The latter leads to relatively warm deep water upwelling to the surface more poleward, which further limits sea ice growth. Those facts explain the significant retreat of sea ice around the Antarctic. Additionally, the upper ocean water becomes a bit saltier from the control run through GMv1, GMv2, to GM with the increasing mixing coefficients, which works to enhance the upward mixing of the warm underlying deep water into the mixed layer as well, further limiting the ability of the ocean to maintain sea ice (not shown). Larger mixing coefficients tend to result in strong vertical stratification in the intermediate and deep levels between 55°S and 70°S in the Southern Ocean and thus reduces the convective mixing there. Although the GM scheme dramatically reduces the sea ice in the Antarctic, compared with Levitus 94, the ocean temperature structure of the GM scheme is more realistic than that of the others, especially with respect to the simulation of the proper spread of relatively warm deep water into the Weddell Sea, which is a key region in the global thermohaline circulation and shows the highest degree of covariability with the extrapolar climate [*Yuan and Martinson*, 2000].

[28] The annual mean Atlantic meridional mass stream function of the control run and differences resulting from the GM scheme and associated mixing coefficient specifications supports the decreases in oceanic heat transports in the Arctic. As shown in Figure 9, the North Atlantic Deep Water (NADW) and Antarctic Bottom Water (AABW) weaken by a magnitude of 2 to 4 Sv (1 Sv = 10^6 m^2/s) from the control run through GMv1, GMv2, to GM. In the Southern Ocean the gradually decreasing slope of the isotherms from the control run through GMv1, GMv2, to GM tends to result in the aforementioned strong vertical stratification and weak convection in the intermediate and deep levels, which lead to gradually weakening AABW. In GM case in the Southern Hemisphere the flattened isotherms in the Southern Ocean dominate the weakened upwelling, which leads the poleward spread of warm water and limits sea ice growth. In the Northern Hemisphere the reduced oceanic overturning (NADW) and atmospheric heat transports play a larger role than the increased poleward isopycnal heat transports, which leads to more sea ice in the Arctic. These explain the asymmetry sea ice changes in each hemisphere.

4.2.2. Wajsowicz Viscosity Diffusion

[29] Coarse resolution ocean models require frictional dissipation in order to suppress instabilities such as those associated with the grid Reynolds number. Subgrid scale dissipation of the momentum in the large-scale ocean models is commonly parameterized as viscous diffusion resulting from the divergence of a stress tensor $\sigma = k_v \cdot \nabla\vec{v}$, where k_v is viscosity coefficient (k_v = max ($\rho_0\beta(\min(\Delta x, \Delta y) \cdot \sqrt{3}/\pi)^3$, 10^8)) and $\vec{v}$ is horizontal velocity. Wajsowicz proposed a formulation of the stress tensor allowing nonconstant viscosity [*Wajsowicz*, 1993]. Its formulation is consistent with the requirement that pure rotation does not produce a stress in the fluid. The GISS ocean component previously employed an alternating binomial filter [*Shapiro*, 1970] in the momentum equations to suppress the horizontal grid alternating patterns in velocity fields in the regions of mass variations (near coast lines and the poles), which is an artifact of C grid schemes and not of the physical flow. In this study the Wajsowicz viscosity diffusion (hereafter referred as WV) is applied to the momentum equations in the GISS coupled model to describe the subgrid scale dissipation and suppress the alternating pattern in a more

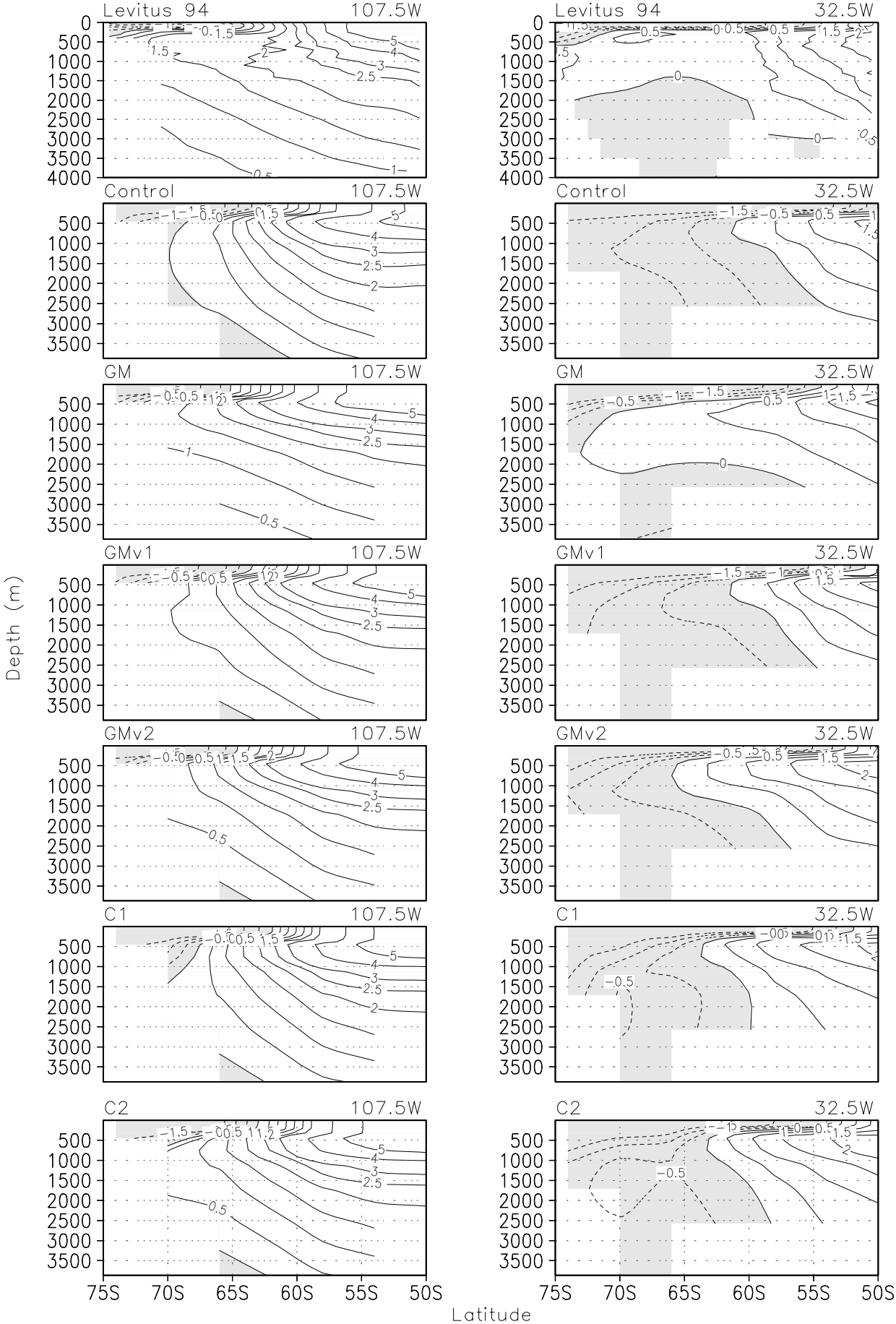
Levitus 94
107.5W
Levitus 94
32.5W
Control
107.5W
Control
32.5W
GM
107.5W
GM
32.5W
GMv1
107.5W
GMv1
32.5W
GMv2
107.5W
GMv2
32.5W
C1
107.5W
C1
32.5W
C2
107.5W
C2
32.5W
Depth (m)
0
500
1000
1500
2000
2500
3000
3500
4000
75S
70S
65S
60S
55S
50S
Latitude

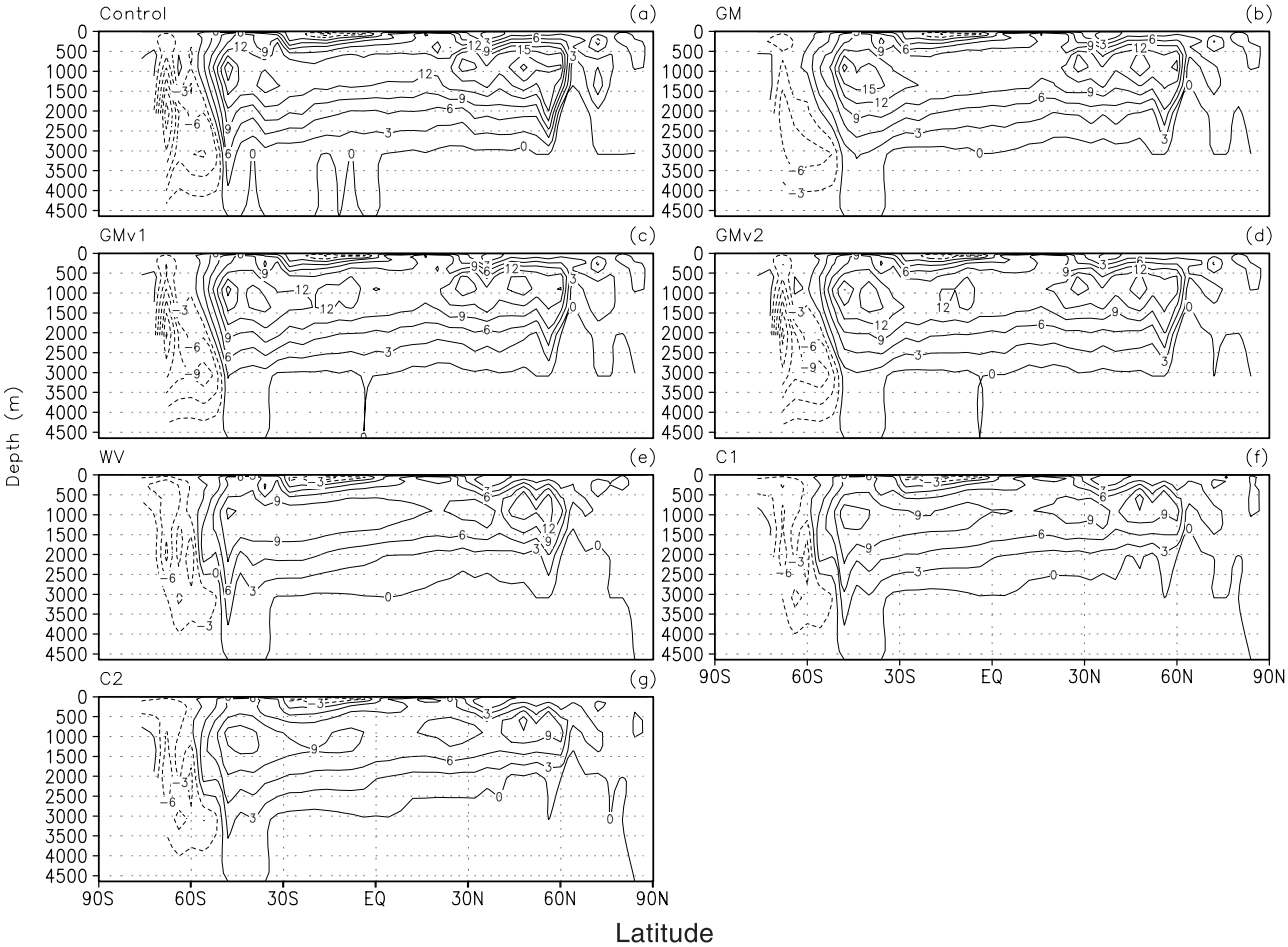

Figure 9. The annual mean Atlantic meridional mass stream function (Sv) for the (a) control, (b) GM, (c) GMv1, (d) GMv2, (e) WV, (f) C1, and (g) C2 runs. Contour interval is 3Sv.

physically meaningful way, and its impacts on the sea ice simulations are presented here.

[30] Compared with the control run, the WV case exhibits an enlargement of sea ice for almost the whole Arctic in February (Figure 4) and September (not shown), with a maximum (~30%) in the GIN seas and North Pacific in February, and in the GIN and Barents Seas and Hudson and Baffin Bays and along the coastlines of the western Eurasian basin in September. Sea ice cover increases within ice packs around the Antarctic (except between the Atlantic and Indian sector of the Antarctic) and decreases in the northern Weddell and Ross Sea in February (Figure 5). The annual mean sea ice thickness increases for the entire Arctic, with a maximum (~1.2 m) in the Barents Sea in the WV run (Figure 6). In the Antarctic there is a thickening of sea ice within ice packs and a thinning of sea ice in the extreme northern Weddell and Ross Sea relative to the control run (Figure 7).

[31] The dramatic sea ice increases in the WV case are the result of a combination of the changes in vertical profiles and meridional heat transports of both the ocean and atmosphere. Figure 10 shows the observed [*Levitus and Boyer*, 1994; *Levitus et al.*, 1994] and simulated February vertical temperature and salinity distribution along 2.5°E in the Arctic. The upper ocean water becomes slightly colder and much fresher, which enhances the ability of the ocean to generate more sea ice there. Additionally, this cold and fresh water atop spreads about 5–10 degrees equatorward in the GIN Seas in the WV run relative to that of the control run, which greatly reduces the contribution of heat from the warm north Atlantic water into the GIN Seas and further facilitates the production of more and thicker sea ice there in February. In the Antarctic the WV run tends to make the upper ocean water fresher and move fresh water southward at the upper level in the Bellingshausen, Amundsen and Weddell Seas. These changes help to reduce the buoyancy, and thereby limit ventilation of the relatively warm deep water to the surface, which result in more sea ice there (not shown). Relative to the control run, the poleward oceanic and atmospheric heat transports are reduced by 0.15 and

Figure 8. (opposite) The vertical ocean temperature profiles along 107.5°W (left column, between the Bellingshausen Sea and Amundsen Sea) and 32.5°W (right column, in the Weddell Sea) in September of the Antarctic for the Levitus 94, control, GM, GMv2, GMv1, C1 and C2 runs (the temperature below 0°C is shaded).

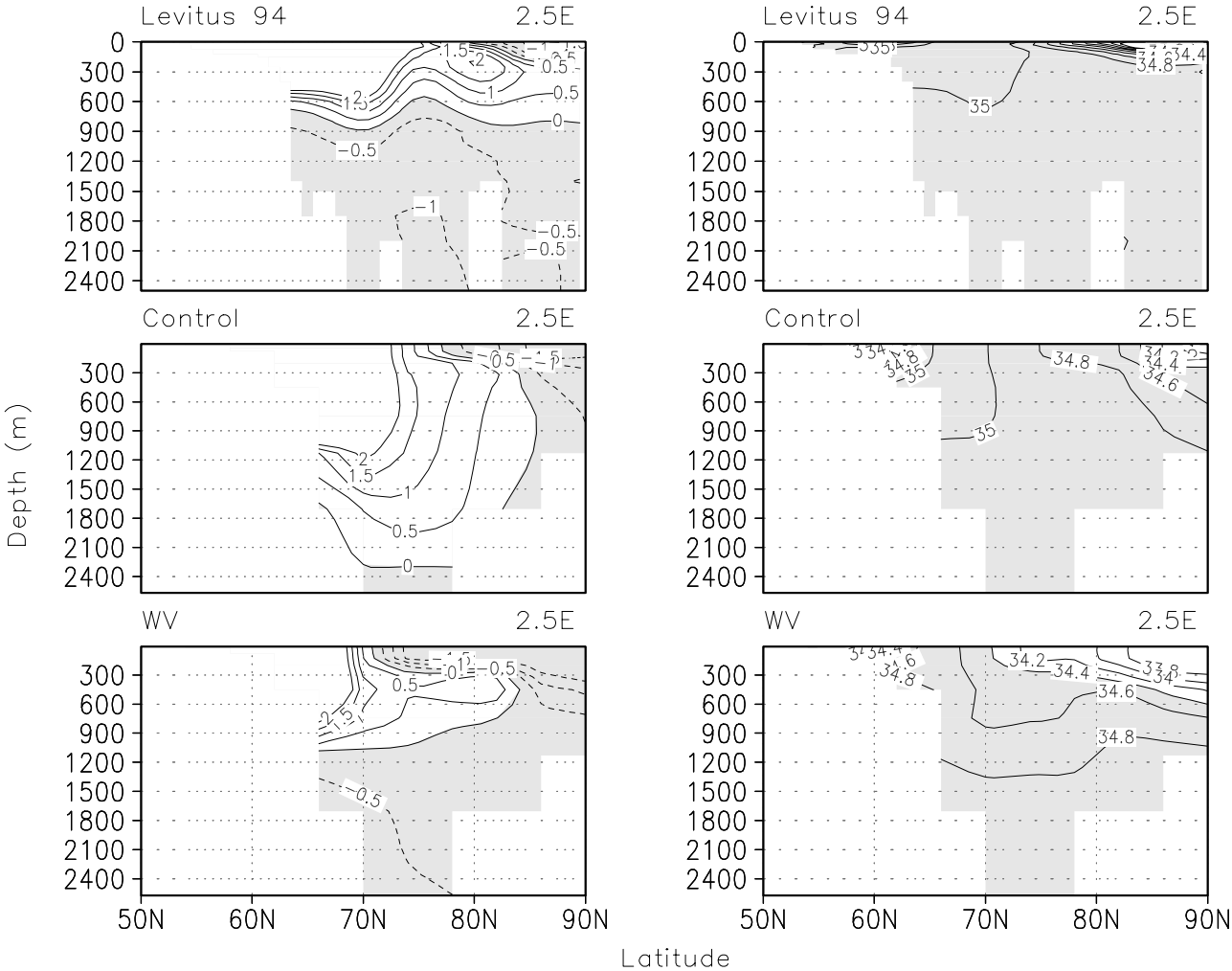

Figure 10. The vertical ocean temperature (left column) and salinity (right column) profiles along 2.5°E (in the GIN Seas) in February of the Arctic for the Levitus 94, control, and WV runs (the temperature below 0°C and salinity above 34.4 ppt are shaded).

0.15 PW, respectively, for north of 52°N, and by 0.03 and 0.04 PW, respectively, for south of 52°S in the WV run.

[32] Since the density of ocean water is primarily controlled by salinity in the cold regions, the fresher upper ocean layer in both hemispheres enhances the vertical stratification and leads to weak convection. Additionally, the downward vertical mass flux in the Arctic and Antarctic in the WV scheme is smaller than that of the control run (not shown). These explain the significant weakening of the NADW, AABW, and Deacon Cell (DC) in the WV run on the magnitude of about 6 Sv compared with the control run (Figure 9).

5. Composite Experiments

[33] Having identified the role of each parameterization in determination of sea ice simulations individually, the next step is to combine these parameterizations. To this end, we ran two extra experiments (C1 and C2, defined as VP + GMv1 + WV and VP + GMv2 + WV, respectively) (Table 1).

[34] In the Arctic the C1 and C2 runs show similar changes in sea ice concentrations relative to the control run. Sea ice cover is reduced in the Labrador and Beaufort Seas in February and increases in other regions in February (Figure 4) and September (not shown). In the Antarctic the C1 run shows a substantial enlargement of sea ice within ice packs around the Antarctic and a reduction of sea ice in the northern Weddell and Ross Seas relative to the control run. While the enlargement of sea ice is confined to the coastlines and the reduction of sea ice occurs in most circumpolar regions in the C2 run. In general, sea ice cover in the C1 run is closer to the observations in the Antarctic (Figure 5).

[35] The C1 and C2 runs show similar sea ice thickness changes in the Arctic. Both increase the annual mean ice thickness by ~1.6 m in the eastern Arctic. However, the C1 and C2 runs still do not improve the ice thickness distribution pattern, which is unfortunately still a common problem in current state-of-the-art global climate models. In the Antarctic the changes of ice thickness in the C1 and C2 runs are similar to their ice cover changes.

[36] The September vertical ocean temperature profile along 107.5°W (between the Bellingshausen Sea and Amundsen Sea) in the C1 and C2 runs show the similarity to that of GMv1 and GMv2, respectively (the slope of

Table 3. Winter and Summer Averaged SAT, Sea Ice Thickness, and Area

	SAT, °C		Thickness, m		Area, 10^6 km^2		SAT, °C		Thickness, m		Area, 10^6 km^2	
	DJF (Arctic winter and Antarctic summer)						*JJA (Arctic summer and Antarctic winter)*					
Run	(45°N–90°N, sea ice and ocean)	(90°S–45°S, sea ice and ocean)	NH	SH	NH	SH	(45°N–90°N, sea ice and ocean)	(90°S–45°S, sea ice and ocean)	NH	SH	NH	SH
Control	−17.27	2.32	1.75	0.16	12.81	4.28	2.44	−4.05	1.76	0.34	9.35	10.66
VP	−20.18	2.23	2.44	0.28	13.47	5.45	2.11	−4.89	2.50	0.42	10.15	12.37
GM	−18.56	3.90	2.06	0.1	12.93	1.47	2.38	−1.64	2.07	0.24	10.	5.02
GMv1	−17.84	2.57	1.84	0.14	13.03	3.73	2.31	−3.64	1.87	0.34	9.66	9.91
GMv2	−18.24	3.31	1.83	0.11	12.85	2.33	2.41	−2.54	1.82	0.29	9.57	7.35
WV	−21.48	2.01	2.31	0.18	14.84	4.99	1.68	−4.57	2.34	0.4	11.48	11.76
C1	−23.36	1.92	3.35	0.33	14.59	6.62	1.80	−5.62	3.52	0.48	11.52	13.84
C2	−22.54	2.37	3.24	0.28	14.57	5.33	1.83	−4.41	3.33	0.43	11.26	11.27
Obs	−18.96	3.09			14.02	4.54	4.21	−7.41			9.1	13.66

isotherms in C1 is steeper than that of C2). Although the GMv1 and GMv2 runs produce different southward warm water spread along 32.5°W, the results in the C1 and C2 runs appear to "split the difference," falling between the GMv1 and GMv2 runs. This indicates the occurrence of nonlinear interactions, in which the VP and/or WV tends to minimize the differences introduced by varying mixing coefficients in the GM scheme. It appears that in particular the run with VP has less sensitivity to changes in subgrid ocean parameterizations. This might be due to simply sea ice in a colder climate (C1/C2 compared with GMv1/GMv2) having a different sensitivity to changes in ocean heat transports.

[37] The C1 and C2 runs reduce the NADW, AABW, and DC by nearly 40% and 50% relative to the control run (~20 Sv, a bit larger than the observations), which is a combination of the results of GMv1 + WV and GMv2 + WV. Also, for north of 52°N, the poleward oceanic and atmospheric heat transports are reduced by 0.16 and 0.17 PW, respectively, in C1 and 0.17 and 0.06 PW, respectively, in C2. For south of 52°S, the poleward oceanic and atmospheric heat transports are reduced by 0.06 and 0.14 PW, respectively, in C1 and 0.05 and 0.14 PW, respectively, in C2.

6. Atmospheric Responses

[38] The most obvious reason for the interest in sea ice sensitivity to these parameterizations is the feedback effect of sea ice on the overall climate sensitivity [*Rind et al.*, 1995]. If sea ice changes substantially, it will influence the surface air temperature (SAT) through its high albedo and strong insulating properties [*Parkinson et al.*, 2001]. Tables 2 and 3 show the annual, winter, and summer averaged SAT in high-latitude north and south (over sea ice and ocean), sea ice thickness, and area of the control run and each experiment. As expected, in general, sea ice and SAT are negatively correlated across the experiments. For example, C1 has almost the most and thickest sea ice in winter and summer for both hemispheres and also has almost the lowest SAT. The following comparisons are relative to the control run. The annual mean SAT of the VP approach cools by 1.83°C and 0.47°C in the high-latitude north and south, respectively, which is mainly contributed by the SAT change in winter associated with an expansion and thickening of sea ice in both high latitudes. The SAT of the GM experiment shows an asymmetric change between hemispheres. There is a slight cooling in the high-latitude north, which mainly results from the expansion and thickening of sea ice and a strong warming in high-latitude south due to the combination of the reduction and thinning of sea ice. The SAT decreases from GM through GMv2 to GMv1 in the southern high-latitude due to the expansion and thickening of sea ice with the reduced mixing coefficients. The winter Arctic and summer Antarctic SAT in the GMv1 and GMv2 runs are comparable to the observations. With the enlargement of sea ice area and the thickening of sea ice in the WV experiment, the winter SAT decreases 4.21 and 0.52°C in the Arctic and Antarctic, respectively. Both composite runs, particularly C1, show a dramatic cooling due to the enlargement and thickening of sea ice in the Arctic and Antarctic relative to other experiments. The winter sea ice area in C1 is closer to the observations relative to the other experiments (Figure 5).

[39] Generally speaking, less (more) sea ice leads to higher (lower) SAT, which leads to the lower (higher) pressure system. In the Northern Hemisphere, as expected, sea level pressure (SLP) and sea ice concentrations are positively correlated from the Hudson Bay east to the Kara Sea with the peak in the GIN seas across each experiment. However, a negative correlation is found in the North Pacific. This suggests that sea ice changes are not a direct determinant of SLP changes in the North Pacific; other factors including changes in temperature gradients, wave propagation, etc. may be important here. Qualitatively speaking, the Aleutian and Icelandic lows, the Beaufort high, and the strong pressure gradient along Fram strait are better represented in C1 relative to the control run, when compared with the observations. In the Southern Hemisphere, by contrast, all experiments exhibit similar SLP patterns to the control run, which suggests that the weak magnitude of both the polar high over the ice cap and the circumpolar lows in the control run are not due to the surface processes analyzed here. Recent research suggests that the poorly resolved stratospheric dynamics in the model may be important. This will be examined in future research (not shown).

7. Discussion and Conclusion

[40] The purpose of this paper is to study the sensitivity of sea ice simulations in the GISS coupled model to sea ice dynamics and subgrid scale ocean processes. The results suggest that sea ice simulations are sensitive to these physical parameterizations to varying degrees (Table 1).

[41] Differences between CF and VP presented in section 4.1 suggest that the absence of resistance to shear stress between sea ice floes produces far too large sea ice drift in both hemispheres. By contrast, VP yields more realistic sea ice properties. It captures the major observed sea ice drift features, improves the simulations of sea ice concentrations, thickness in some regions to some degree, and generates more realistic sea ice export through Fram Strait with reasonable combinations of ice velocities and thickness. Therefore the inclusion of the resistance to shear is an important improvement to sea ice simulations in the global climate model, though these might be a function of the coarser resolution. Compared with moderate ice drift differences (between CF and VP; between CF, VP, and the observations) reported in prior stand-alone or regional modeling studies [*Kreyscher et al.*, 2000], the dramatic differences here suggest a higher sensitivity in global climate models when the different components interact, though these might be a function of the coarser resolution. Additionally, the CPU time consumed in VP [*Zhang and Rothrock*, 2000] is comparable to that consumed in CF and thus there do not appear to be any disadvantages to its use in climate studies.

[42] The results presented in section 4.2 suggest that the GM scheme significantly improves the simulation of vertical temperature characteristics in the Southern Ocean. A major reason for such improvement is that the GM scheme mimics isopycnal mixing contributed by the energetic mesoscale eddies, which extract their energy from the available potential energy of the mean flow and eddy fluxes work to reduce the slope of the isotherms. However, the GM scheme dramatically reduces Antarctic sea ice cover by moving the upper warm water and the zone of weak vertical stability poleward in the Southern Ocean.

[43] In the GM scheme, the main parameters are the isopycnal tracer mixing and thickness diffusion coefficients (here assumed equal). The simulations show that the sea ice and high latitude ocean characteristics are highly sensitive to the specification of the mixing coefficients. In particular, the slope of the isotherms become gradually steeper (diverging from the observations, Figure 8) and Antarctic sea ice extends more equatorward (approaching the observations, Figure 5) as the reduced mixing coefficients from GM through GMv2 to GMv1. Although the mixing coefficients are only positive in the Visbeck specification, in reality it may be locally negative. *Nakamura and Chao* [2000] suggests that k_m has extremely large spatial and temporal variations, with negative values about half of the time. k_m even varies by several order of magnitude from 10 m^2/s to 10^7 m^2/s in the western north Atlantic based on output of an eddy-resolving ocean model. The lack of observational data has prohibited a direct estimation of k_m for the real oceans, especially in high latitudes. The implication of our sensitivity experiments is that the mixing coefficient might be small in the upper and large in the intermediate and deep levels of the Antarctic; such a distribution would generate more realistic sea ice cover and ocean vertical temperature structure. While we have shown some improvements in the simulations due to the GM scheme, finding the appropriate spatial (both horizontal and vertical) and temporal variability of k_m remains an important research priority.

[44] More surprising is the sensitivity of sea ice to the Wajsowicz viscosity diffusion applied in the momentum equations. There is an enlargement and thickening of sea ice in the Arctic especially in the GIN Seas and within ice packs around the Antarctic due to the freshening surface ocean water and reduced poleward oceanic and atmospheric heat transports. The WV scheme reduces the downward vertical mass fluxes and enhances vertical ocean stratification in both hemispheres, thus leading to a significant weakening of the NADW, AABW, and DC by about 6 Sv. In contrast to the WV scheme, *Smagorinsky* [1993] proposed an alternative scheme whereby the value of viscosity is isotropic but spatially varying as a function of the local magnitude of the stress. This scheme will be examined in future sensitivity experiments.

[45] Some of the results in the C1 and C2 runs are approximately the linear combination of the results of VP + GMv1 + WV and VP + GMv2 + WV, respectively. However, the differences between C1 and C2 are much less than the differences between GMv1 and GMv2, indicating that the different processes have nonlinear interactions. Relative to the other individual experiment, their winter sea ice area in the Arctic and Antarctic is closer to the observations. However, both reduce the ocean overturning and poleward oceanic and atmospheric heat transports greatly. Further research into improving the representation of the sea ice thermodynamics is currently being undertaken. This includes the change of the sea ice albedo formulation [*Schramm et al.*, 1997], the inclusion of sea ice salinity and its thermodynamic effects [*Bitz and Lipscomb*, 1999], the specification of the under ice fluxes [*McPhee et al.*, 1987; *Holland and Jenkins*, 1999], and the penetration of solar radiation in sea ice. Preliminary results indicate that further increase in the overturning is likely to occur as a consequence and this will be addressed in the future paper. In conclusion, sea ice is strongly affected by sea ice dynamics and subgrid ocean physical parameterizations. The optimum combination of the effects still remains elusive.

[46] **Acknowledgments.** The authors thank J. Zhang for his explanations of the global ice model version 1. We also thank S. M. Griffies and B. Tremblay for the discussion and J. Hansen for organizing the sea ice workshop in 1999 from which many ideas for future research directions were inspired. The observed sea ice drift used herein were derived by C. Flowler, W. Emery, and J. Maslanik using the SMMR/SSMI satellite data provided by the National Snow and Ice Data Center. This research was supported by the NASA polar programs (622-82-34), and a grants/cooperative agreement form NOAA/CORC (ARCHES Awards: NA17RJ1231 and NA77RJ0453). Lamont-Doherty Earth Observatory Contribution 6401.

References

Aagaard, K., and E. C. Carmack, The role of sea ice and other freshwater in the arctic circulation, *J. Geophys. Res.*, *94*, 14,485–14,498, 1989.

Alexander, R. C., and R. L. Mobley, Monthly average sea-surface temperatures and ice-pack limits on a 1% global grid, *Mon. Weather Rev.*, *104*, 143–148, 1976.

Arakawa, A., and V. R. Lamb, Computational design of the basic dynamical processes of the UCLA general circulation model, *Methods in Computational Physics*, vol. 17, 337 pp., Academic, San Diego, Calif., 1977.

Bitz, C., and W. H. Lipscomb, An energy-conserving thermodynamic model of sea ice, *J. Geophys. Res.*, *104*, 15,669–15,677, 1999.

Bitz, C., et al., Sea ice response to wind forcing from AMIP models, paper presented at Conf. on Polar Meteorol. and Oceanogr., Am. Meteorol. Soc., Boston, Mass., 2001.

Bourke, R. H., and R. P. Garrett, Sea-ice thickness distribution in the Arctic Ocean, *Cold Reg. Sci. Technol.*, *13*, 259–280, 1987.

Bryan, K., J. K. Dukowicz, and R. D. Smith, On the mixing coefficient in the parameterization of bolus velocity, *J. Phys. Oceanogr.*, *29*, 2442–2456, 1999.

Danabasoglu, G., and J. C. McWilliams, Sensitivity of the global ocean circulation to parameterizations of mesoscale tracer transports, *J. Climate*, *8*, 2967–2987, 1995.

Danabasoglu, G., J. C. McWilliams, and P. R. Gent, The role of mesoscale tracer transports in the global ocean circulation, *Science*, *264*, 1123–1126, 1994.

Flato, G. M., and G. J. Boer, Warming asymmetry in climate change simulations, *Geophys. Res. Lett.*, *28*, 195–198, 2001.

Flato, G. M., and W. D. Hibler, Modeling pack ice as a cavitating fluid, *J. Phys. Oceanogr.*, *96*, 4589–4603, 1992.

Gates, W. L., et al., Climate models—Evaluation. *Climate Change 1995*, edited by J. T. Houghton et al., pp. 233–284, Cambridge Univ. Press, New York, 1996.

Gent, P. R., and J. C. McWilliams, Isopycnal mixing in ocean circulation models, *J. Geophys. Res.*, *20*, 150–155, 1990.

Gent, P. R., J. Willebrand, T. J. McDougall, and J. C. McWilliams, Parameterizing eddy-induced tracer transports in ocean circulation models, *J. Phys. Oceanogr.*, *25*, 463–474, 1995.

Griffies, S. M., A. Gnanadesikan, R. C. Pacanowski, V. Larichev, J. K. Dukowicz, and R. D. Smith, Isoneutral diffusion in a z-coordinate ocean model, *J. Phys. Oceanogr.*, *28*, 805–830, 1998.

Hansen, J., G. Russell, D. Rind, P. Stone, A. Lacis, S. Lebedeff, R. Ruedy, and L. Travis, Efficient three-dimensional global models for climatic studies: Models I and II, *Mon. Weather Rev.*, *111*, 609–662, 1983.

Harder, M., P. Lemke, Modeling the extent of sea ice ridging in the Weddell Sea, in *The Polar Oceans and Their Role in Shaping the Global Environment*, *Geophys. Monogr. Ser.*, vol. 85, pp. 187–197, AGU, Washington, DC, 1994.

Harder, M., P. Lemke, and M. Hilmer, Simulation of sea ice transport through Fram Strait: Natural variability and sensitivity to foring, *J. Geophys. Res.*, *103*, 5595–5606, 1998.

Held, I. M., and V. D. Larichev, A scaling theory for horizontally homogeneous, baroclinically unstable flow on a beta plane, *J. Atmos. Sci.*, *36*, 1844–1861, 1996.

Hibler, W. D., A dynamic thermodynamic sea ice model, *J. Phys. Oceanogr.*, *9*, 815–846, 1979.

Hibler, W. D., Role of sea ice dynamics in modeling CO_2 increase, in *Climate and Climate Sensitivity*, *Geophys. Monogr. Ser.*, vol. 29, edited by J. E. Hansen and T. Takahashi, pp. 238–253, AGU, Washington, DC, 1984.

Hibler, W. D., and E. M. Schulson, On modeling sea-ice fracture and flow in numerical investigations of climate, *Ann. Glaciol.*, *25*, 26–32, 1997.

Hilmer, M., M. Harder, and P. Lemke, Sea ice transport: A highly variable link between Arctic and North Atlantic, *Geophys. Res. Lett.*, *25*, 26–32, 1997.

Holland, D. M., and A. Jenkins, Modeling thermodynamic ice-ocean interactions at the base of an ice shelf, *J. Clim.*, *12*, 1787–1800, 1999.

Intergovernmental Panel on Climate Change (IPCC), *Climate Change 1995: The Science of Climate Change*, edited by J. T. Houghton et al., Cambridge Univ. Press, New York, 1996.

Kattenberg, A., et al., Climate models—Projections of future climate, in *Climate Change 1995*: *The Science of Climate Change*, edited by J. T. Houghton et al., 572 pp., Cambridge Univ. Press, New York, 1996.

Kreyscher, M., M. Harder, P. Lemke, and G. M. Flato, Results of the sea ice model intercomparison project: Evaluation of sea-ice rheology schemes for use in climate simulations, *J. Geophys. Res.*, *105*, 11,299–11,320, 2000.

Kwok, R., and D. A. Rothrock, Variability of Fram Strait ice flux and North Atlantic Oscillation, *J. Geophys. Res.*, *104*, 5177–5189, 1999.

Large, W. G., J. C. McWilliams, and S. C. Doney, Oceanic vertical mixing: a review and a model with a nonlocal boundary layer parameterization, *Rev. Geophys.*, *32*, 363–403, 1994.

Lemke, P., M. Harder, and M. Hilmer, The response of Arctic sea ice to global change, *Clim. Change*, *46*, 277–287, 2000.

Levitus, S., and T. P. Boyer, *World Ocean Atlas 1994*, vol. 4, *Temperature*, 117 pp., U.S. Dep. of Comm., Washington, DC, 1994.

Levitus, S., R. Burgett, and T. P. Boyer, *World Ocean Atlas 1994*, vol. 3, *Salinity*, 99 pp., U.S. Dep. of Comm., Washington, DC, 1994.

Liu, J., D. Martinson, X. Yuan, and D. Rind, Evaluating Antarctic sea ice variability and its teleconnections in global climate models, *Int. J. Climatol.*, *22*, 885–900, 2002.

Martinson, D. G., Evolution of the Southern Ocean winter mixing layer and sea ice: Open ocean deepwater formation and ventilation, *J. Geophys. Res.*, *95*, 11,641–11,654, 1990.

Martinson, D. G., and M. Steele, Future of the Arctic sea ice cover: Implications of an Antarctic analog, *Geophys. Res. Lett.*, *28*, 307–310, 2001.

McPhee, M. G., G. A. Maykut, and J. H. Morison, Dynamics and thermodynamics of the ice/upper ocean system in the marginal ice zone of the Greenland Sea, *J. Geophys. Res.*, *92*, 7017–7031, 1987.

Miller, J., and G. Russell, Projected impact of climate change on the freshwater and salt budgets of the Arctic ocean by a global climate model, *Geophys. Res. Lett.*, *27*, 1183–1186, 2000.

Miller, J. R., G. L. Russell, and G. Caliri, Continental scale river flow in climate models, *J. Clim.*, *7*, 914–928, 1994.

Nakamuka, M., and Y. Chao, On the eddy isopycnal thickness diffusivity of the Gent-McWilliams subgrid mixing parameterization, *J. Clim.*, *13*, 502–510, 2000.

Parkinson, C. L., D. Rind, R. J. Healy, and D. Martinson, The impact of sea ice concentration accuracies on climate model simulations with the GISS GCM, *J. Clim.*, *14*, 2606–2623, 2001.

Pollard, D., and S. L. Thompson, Sea-ice dynamics and CO_2 sensitivity in global climate models, *Atmos. Ocean*, *32*, 449–467, 1994.

Randall, D., J. Curry, D. Battisti, G. Flato, R. Grumbine, S. Hakkinen, D. Martinson, R. Preller, J. Walsh, and J. Weatherly, Status of and outlook for the large scale modeling of atmosphere-ice-ocean interactions in the Arctic, *Bull. Am. Meteorol. Soc.*, *79*, 197–219, 1998.

Rind, D., R. Healy, C. Parkinson, and D. Martinson, The role of sea ice in $2 \times CO_2$ climate model sensitivity, I, The total influence of sea ice thickness and extent, *J. Clim.*, *8*, 449–463, 1995.

Russell, G. L., and J. A. Lerner, A new finite differencing scheme for the tracer transport equation, *J. Appl. Meteorol.*, *20*, 1483–1498, 1981.

Russell, G. L., J. R. Miller, and D. Rind, A coupled atmosphere-ocean model for transient climate change studies, *Atmos. Ocean*, *33*, 683–730, 1995.

Russell, G. L., J. R. Miller, D. Rind, R. A. Ruedy, G. A. Schmidt, and S. Sheth, Comparison of model and observed regional temperature changes during the past 40 years, *J. Geophys. Res.*, *105*, 14,891–14,898, 2000.

Schmitz, W. J., On the world ocean circulation, vol. I, Some global features/North Atlantic circulation, *Tech. Rep. WHOI-96-03*, 141 pp., Woods Hole Oceanogr. Inst., Woods Hole, Mass., 1996.

Schramm, J. L., M. M. Holland, and J. A. Curry, Modeling the thermodynamics of a sea ice thickness distribution, 1, Sensitivity to ice thickness resolution, *J. Geophys. Res.*, *102*, 23,079–23,091, 1997.

Shapiro, R., Smoothing, filtering and boundary effects, *Rev. Geophys.*, *8*, 359–387, 1970.

Smagorinsky, J., *Some Historical Remarks on the Use of Nonlinear Viscosity in Large Eddy Simulation of Complex Engineering and Geophysical Flows*, Cambridge Univ. Press, New York, 1993.

Steele, M., and T. Boyd, Retreat of the cold halocline layer in the Arctic Ocean, *J. Geophys. Res.*, *103*, 10,419–10,435, 1998.

Visbeck, M., J. Marshall, T. Haine, and M. Spall, On the specification of eddy transfer coefficients in coarse resolution ocean circulation models, *J. Phys. Oceanogr.*, *27*, 381–402, 1997.

Walsh, J. E., The role of sea ice in climate variability: Theories and evidence, *Atmos. Ocean*, *21*, 229–242, 1983.

Walsh, J. E., and C. Johnson, An analysis of Arctic sea ice fluctuations, *J. Phys. Oceanogr.*, *9*, 580–591, 1979.

Wajsowicz, R. C., A consistent formulation of the anisotropic stress tensor for use in models of the large-scale ocean circulation, *J. Comput. Phys.*, *105*, 333–338, 1993.

Weatherly, J. W., and Y. Zhang, The response of the polar regions to increased CO_2 in a global climate model with elastic-viscous-plastic sea ice, *J. Clim.*, *14*, 268–283, 2001.

Weatherly, J. W., B. P. Briegleb, W. G. Large, and J. A. Maslanik, Sea ice and polar climate in the NCAR CSM, *J. Clim.*, *11*, 1472–1486, 1998.

Yuan, X., and D. G. Martinson, Antarctic sea ice variability and its global connectivity, *J. Clim.*, *13*, 1697–1717, 2000.

Zhang, J., and W. D. Hibler III, On an efficient numerical method for modeling sea ice dynamics, *J. Geophys. Res.*, *102*, 8691–8702, 1997.

Zhang, J., and D. Rothrock, Modeling Arctic sea ice with an efficient plastic solution, *J. Geophys. Res.*, *105*, 3325–3338, 2000.

J. Liu, NASA/Goddard Space Flight Center, Institute for Space Studies, 2880 Broadway, New York, NY 10025, USA. (jliu@giss.nasa.gov)

D. G. Martinson, Lamont-Doherty Earth Observatory of Columbia University, Palisades, NY 10964, USA. (dgm@ldeo.columbia.edu)

G. A. Schmidt, D. Rind, and G. L. Russell, NASA Goddard Institute for Space Studies, New York, NY 10025, USA. (gschmidt@giss.nasa.gov; drind@giss.nasa.gov; grussell@giss.nasa.gov)